Supplement of Ocean Sci., 22, 653–678, 2026
https://doi.org/10.5194/os-22-653-2026-supplement

Ocean Science Open Access EGU

Supplement of

Characteristics of ocean mesoscale eddies in the Canadian Basin from a high resolution pan-Arctic model

Noémie Planat et al.

Correspondence to: Noémie Planat (noemie.planat@mail.mcgill.ca)

Supplement

List of figures:

- Fig S1 : Rossby radius in CREG12
- Fig. S2 (Sept.) and S3 (March) : Temporal evolution of the sea ice concentration and extent in CREG12, NSIDC (sea ice concentration) and PIOMAS (sea ice thickness)
- Fig. S4 : Fresh water content in CREG compared to observations
- Fig. S5 : Mean Kinetic Energy from CREG12 and from mooring estimates of von Appen et al. (2022)
- Fig. S6 : Mooring-like kinetic energy from CREG12 in the Beaufort Gyre
- Fig. S7 : Sensitivity to method's parameters α
- Fig. S8 : Changes of eddy properties simultaneously along 2 properties
- Fig. S9 : Hovmöller diagram of a latitudinal section of eddy density and duration
- Fig. S10 : Change in eddy properties through the 26 years.
- Fig. S11 : Time series of eddy generation for the different sea ice concentration (sic) categories: Open Ocean (sic $< 0.15\%$), MIZ ($0.15\% <$sic$< 0.8\%$) and Pack ice (sic$> 0.8\%$)
- Fig. S12: Long-lived eddy population density time series
- Fig. S13 : Spatial repartition of ITPs across the CB between 2003 and 2024
- Fig. S14 : Long-lived eddies characteristics histogram

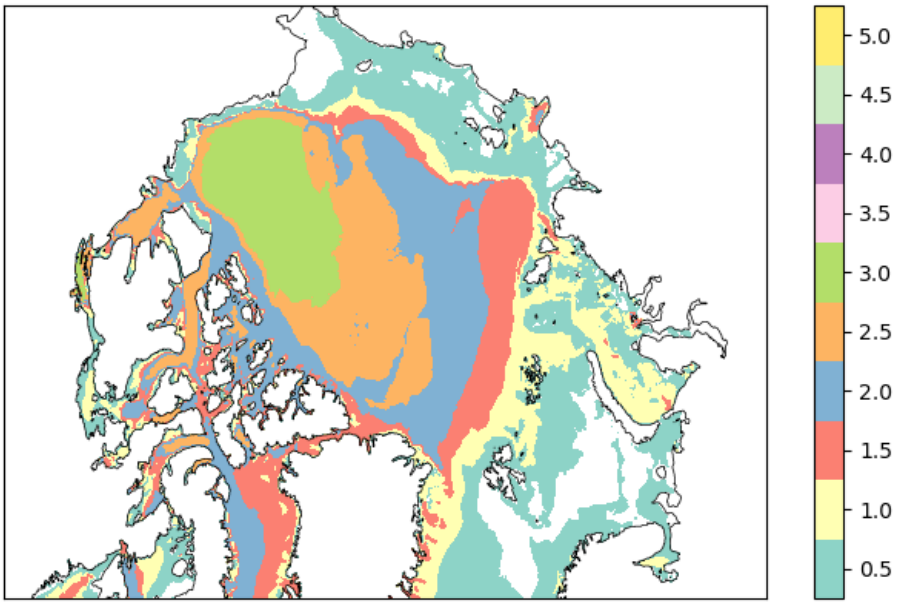

Figure S1. Ratio of the first baroclinic Rossby radius of deformation R_o in the simulation to the maximal grid spacing ds in the simulation. R_o is computed from the simplified equation introduced by Chelton et al. (1998) and compared with the exact formulation in the Arctic Ocean by Nurser and Bacon (2013). Computations are done from daily calculations of the Brunt-Vaisala frequency (N^2) averaged over 26 years. ds is taken at each grid point as the maximum between dx and dy.

References

Chelton, D. B., deSzoeke, R. A., Schlax, M. G., El Naggar, K., and Siwertz, N.: Geographical Variability of the First Baroclinic Rossby Radius of Deformation, Journal of Physical Oceanography, 28, 433–460, https://doi.org/10.1175/1520-0485(1998)028<0433:GVOTFB>2.0.CO;2, 1998.

Meneghello, G., Marshall, J., Lique, C., Isachsen, L. E., Doddridge, E., Campin, J.-M., Regan, H., and Talandier, C.: Genesis and Decay of Mesoscale Baroclinic Eddies in the Seasonally Ice-Covered Interior Arctic Ocean, JOURNAL OF PHYSICAL OCEANOGRAPHY, 51, 2021.

Nurser, A. J. G. and Bacon, S.: Arctic Ocean Rossby radius Eddy length scales and the Rossby radius in the Arctic Ocean Arctic Ocean Rossby radius, Ocean Sci. Discuss, 10, 1807–1831, https://doi.org/10.5194/osd-10-1807-2013, 2013.

Proshutinsky, A., Krishfield, R., Timmermans, M.-L., Toole, J., Carmack, E., McLaughlin, F., Williams, W. J., Zimmermann, S., Itoh, M., and Shimada, K.: Beaufort Gyre freshwater reservoir: State and variability from observations, 2009.

Toole, J., Krishfield, R., Timmermans, M.-L., and Proshutinsky, A.: The Ice-Tethered Profiler: Argo of the Arctic, Oceanography, 24, 126–135, https://doi.org/10.5670/oceanog.2011.64, 2011.

von Appen, W.-J., Baumann, T. M., Janout, M. A., Koldunov, N. V., Lenn, Y.-D., Pickart, R. S., and Wang, Q.: Eddies and the Distribution of Eddy Kinetic Energy in the Arctic Ocean, 35, 42–51, 2022.

Zhang, J. and Rothrock, D. A.: Modeling Global Sea Ice with a Thickness and Enthalpy Distribution Model in Generalized Curvilinear Coordinates, Monthly Weather Review, 131, 845–861, https://doi.org/10.1175/1520-0493(2003)131<0845:MGSIWA>2.0.CO;2, 2003.

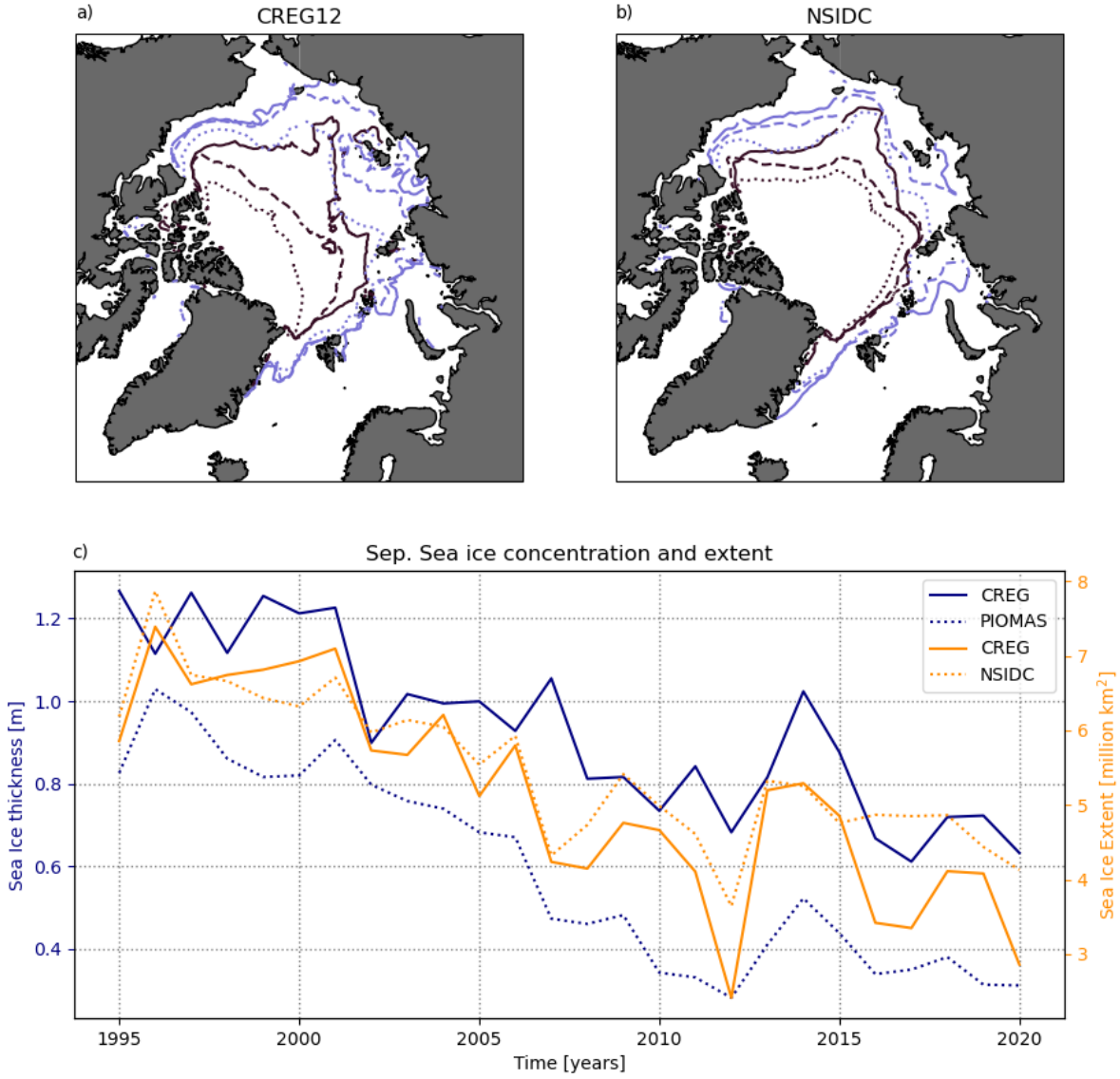

Figure 2. Evolution of the ice concentration in September in CREG12 (a) and NSIDC concentration dataset (b) between 1995-2000 (plain lines), 2000-2010 (dashed lines) and 2010-2020 (dotted lines). Pink and purple respectively represent the 0.15 and 0.80 concentration isolines. (c) Sea ice thickness (blue) and extent (orange) for CREG (plain lines), NSIDC (dotted orange) PIOMAS Arctic Sea Ice Volume Reanalysis (Zhang and Rothrock, 2003) (dotted blue) across the 26 years of simulation.

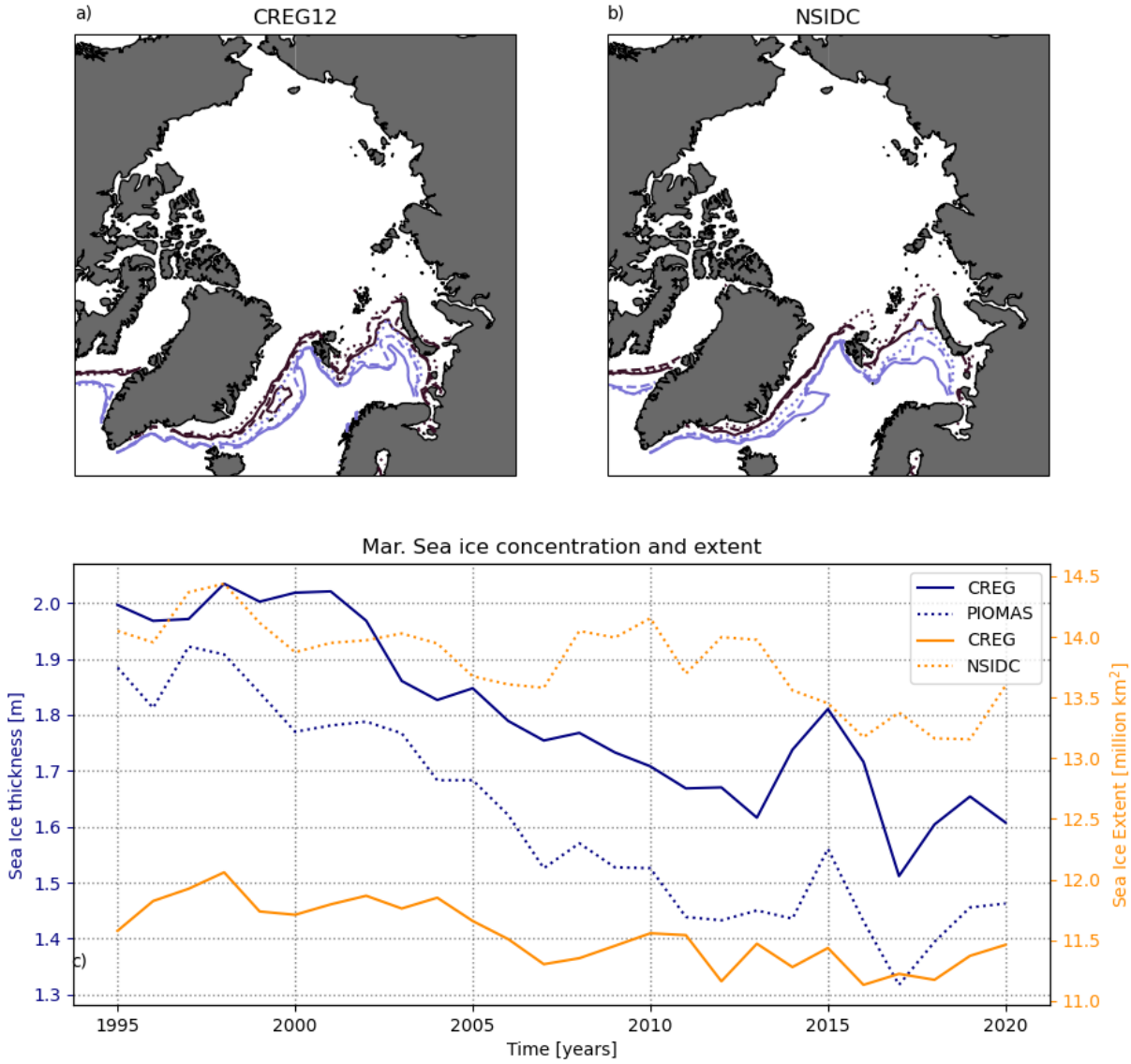

Figure 3. Same as Fig. 2 in March.

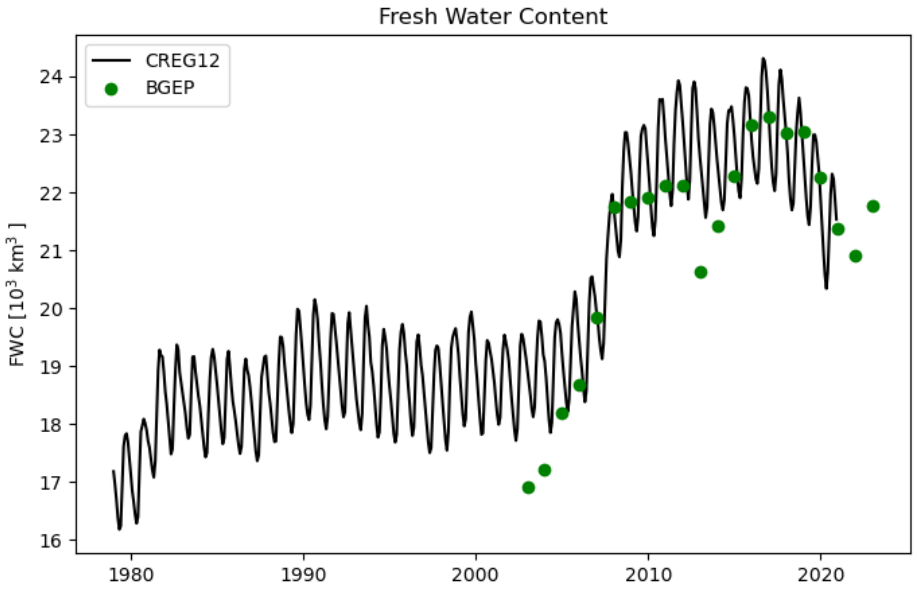

Figure 4. Fresh water content from CREG computed over the domain $130°W - 170°W, 70.5°N - 80.5°N$, referenced to 34.8 psu. Green dots show observation-derived estimates of the fresh water content in the same area (Proshutinsky et al., 2009).

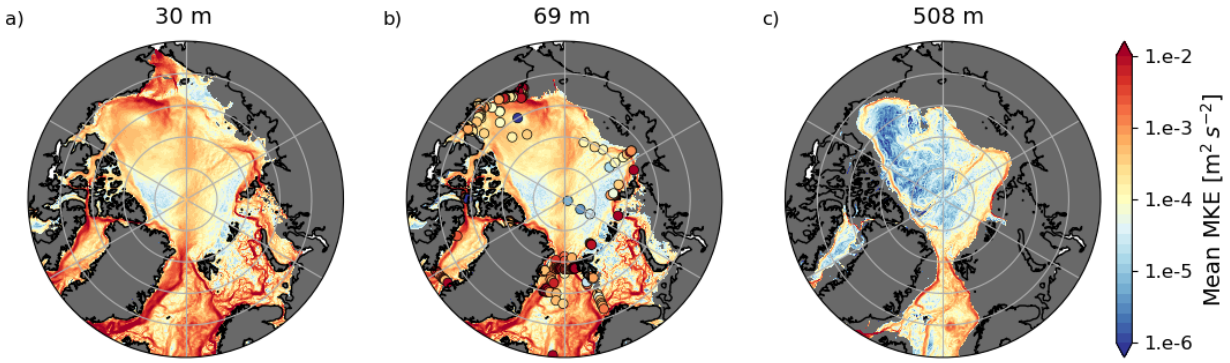

Figure 5. Mean Kinetic Energy (MKE) computed from monthly averages and averaged over the 26 years of simulation (a) within the surface layer at 30 m, (b) within the halocline at 69 m and (c) within the AW layer at 508 m. Super-imposed on (b) are mooring estimates of MKE from von Appen et al. (2022) computed for depths between 50-100 m, corresponding to monthly deviations. The reader is refered to this paper for details on the calculations.

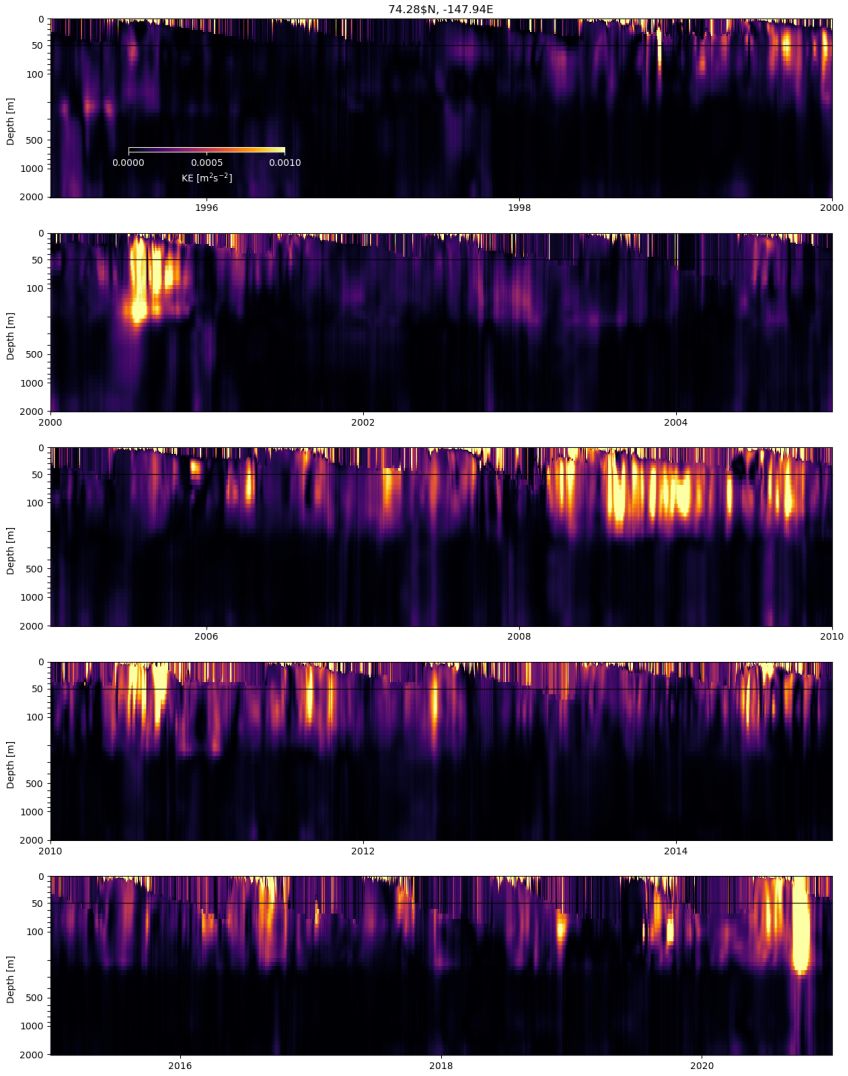

Figure 6. Kinetic energy at 74.28°N, 147.94°W (close to the localisation of mooring A from the Beaufort Gyre Exploration Project) from Jan. 1995 to Dec. 2020. Note the linear vertical axis for the upper 50 m and the logarithmic vertical scale between 50 and 2000 m. Similar to Fig. A1 from Meneghello et al. (2021), we show surface intensified structures, and deeper structures spanning the AW layer (although weaker).

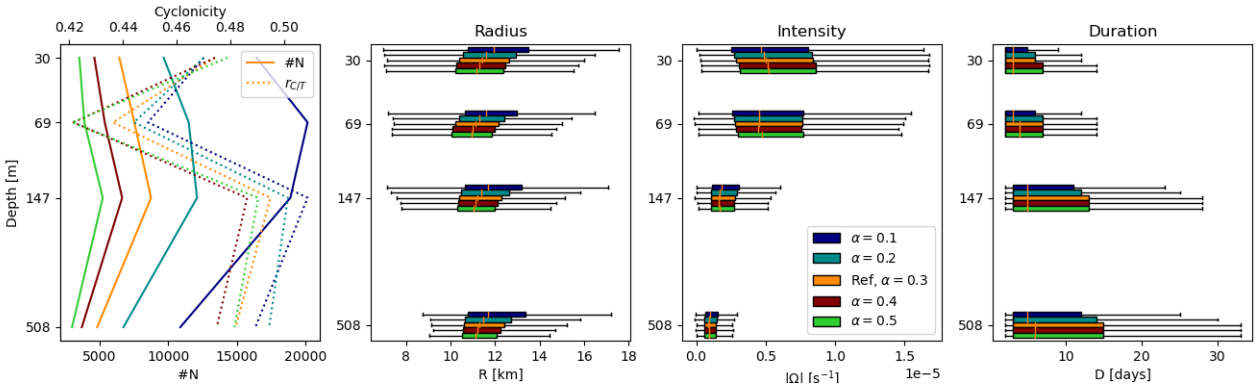

Figure 7. (a) polarity (dotted lines) and number of eddies detected (plain lines); median and 90/10-th percentiles for (b) the radius, (c) the intensity (absolute value of vorticity Ω) and (d) the duration when varying the detection parameter α from 0.2 to 0.5. Sensibility is assessed at 35 m, 69 m, 120 m, 200 m and 550 m for one year (chosen randomly as 2001) and for the whole Canadian Basin.

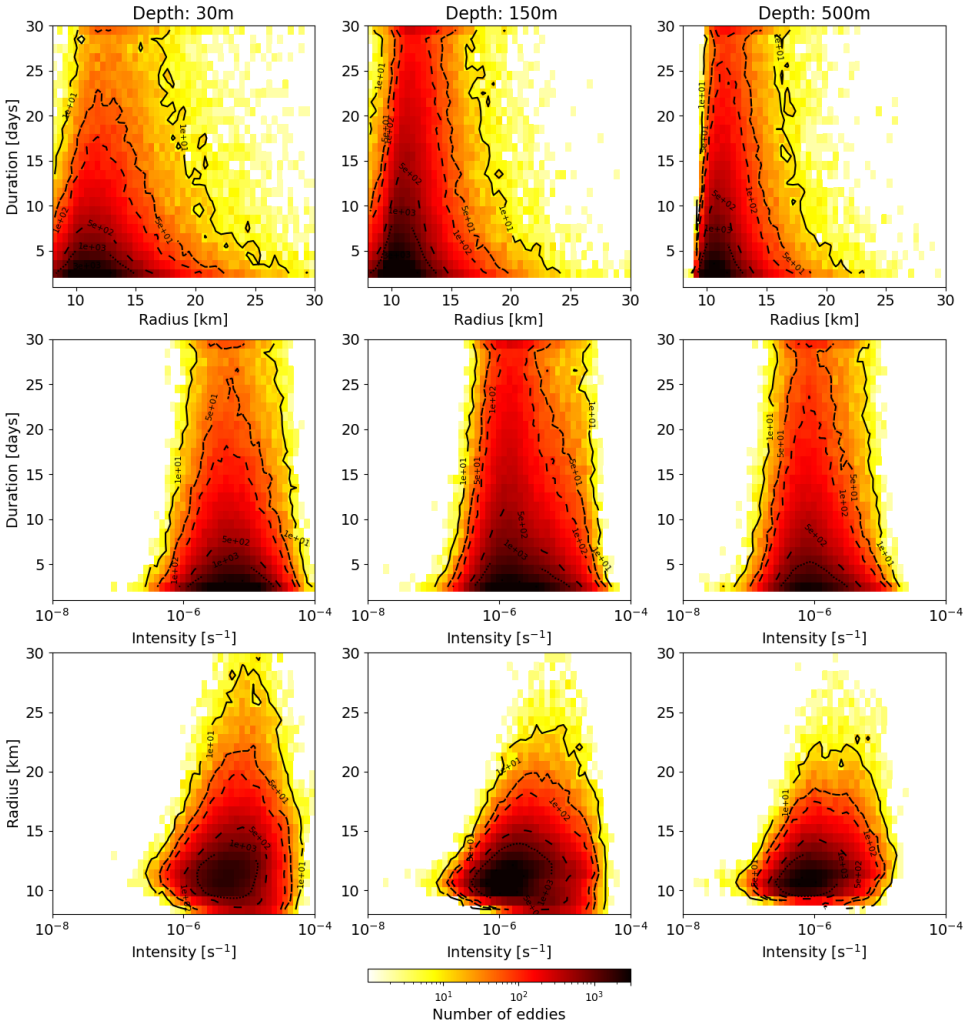

Figure 8. Histogram of duration, intensity and radius simultaneously at 30 m (first column), 150 m (second column) and 500 m (last column). First row display duration *vs* radius, second row duration *vs* intensity and last row radius *vs* intensity. Plain, dashed, loosely dashed, very loosely dashed and dotted lines indicate iso-contours of 10, 50, 100, 500 and 1000 eddies.

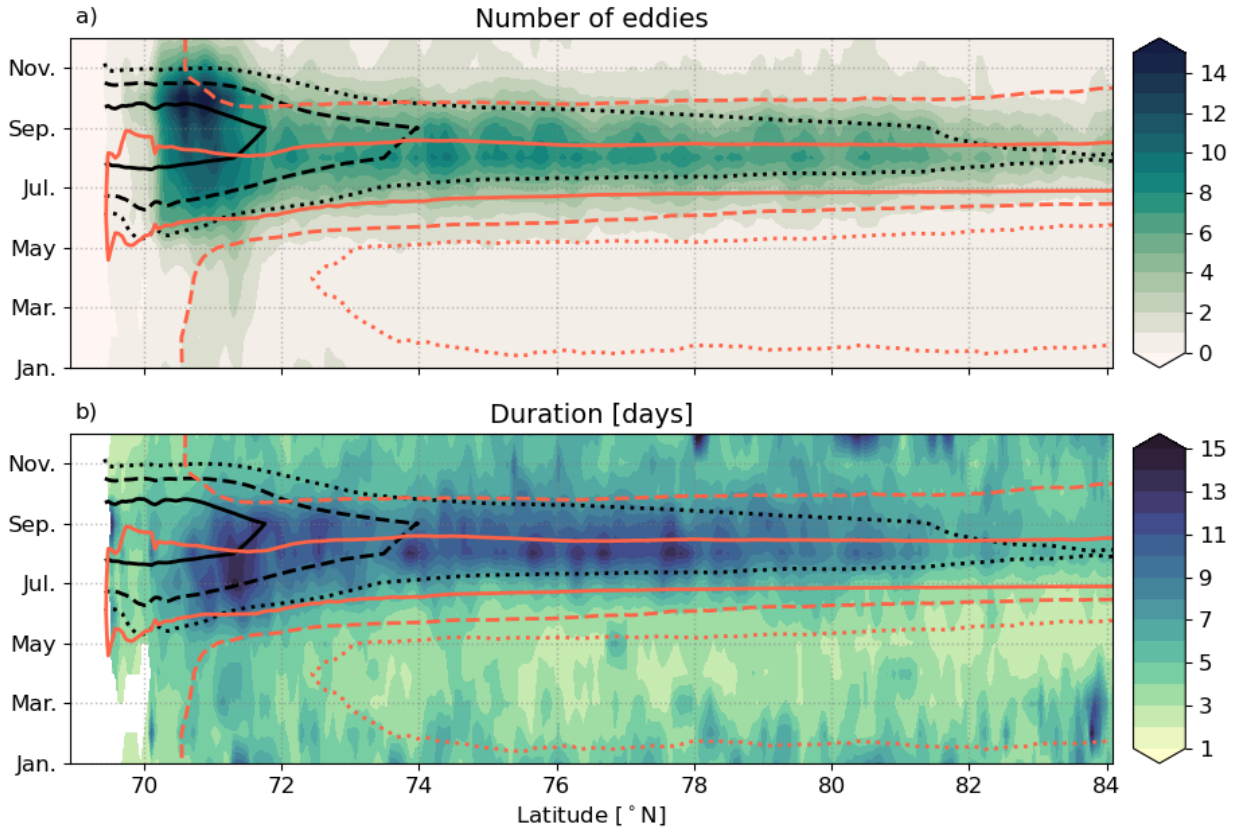

Figure 9. Hovmöller diagram of a latitudinal section from the Alaskan shelf to the center of the Arctic (see red line on Fig. 1 of the main manuscript) against seasons for (a) the total number of eddies detected over the 26 years and (b) eddy duration. Both fields are summed or averaged zonally across a band of 150 km and vertically averaged within the upper layer (from surface to 85 m). Black plain, dashed and dotted lines indicate the 0.15, 0.5 and 0.8 sea ice fraction. Orange plain, dashed and dotted lines indicate the 5 m, 20 m and 40 m mixed layer depth.

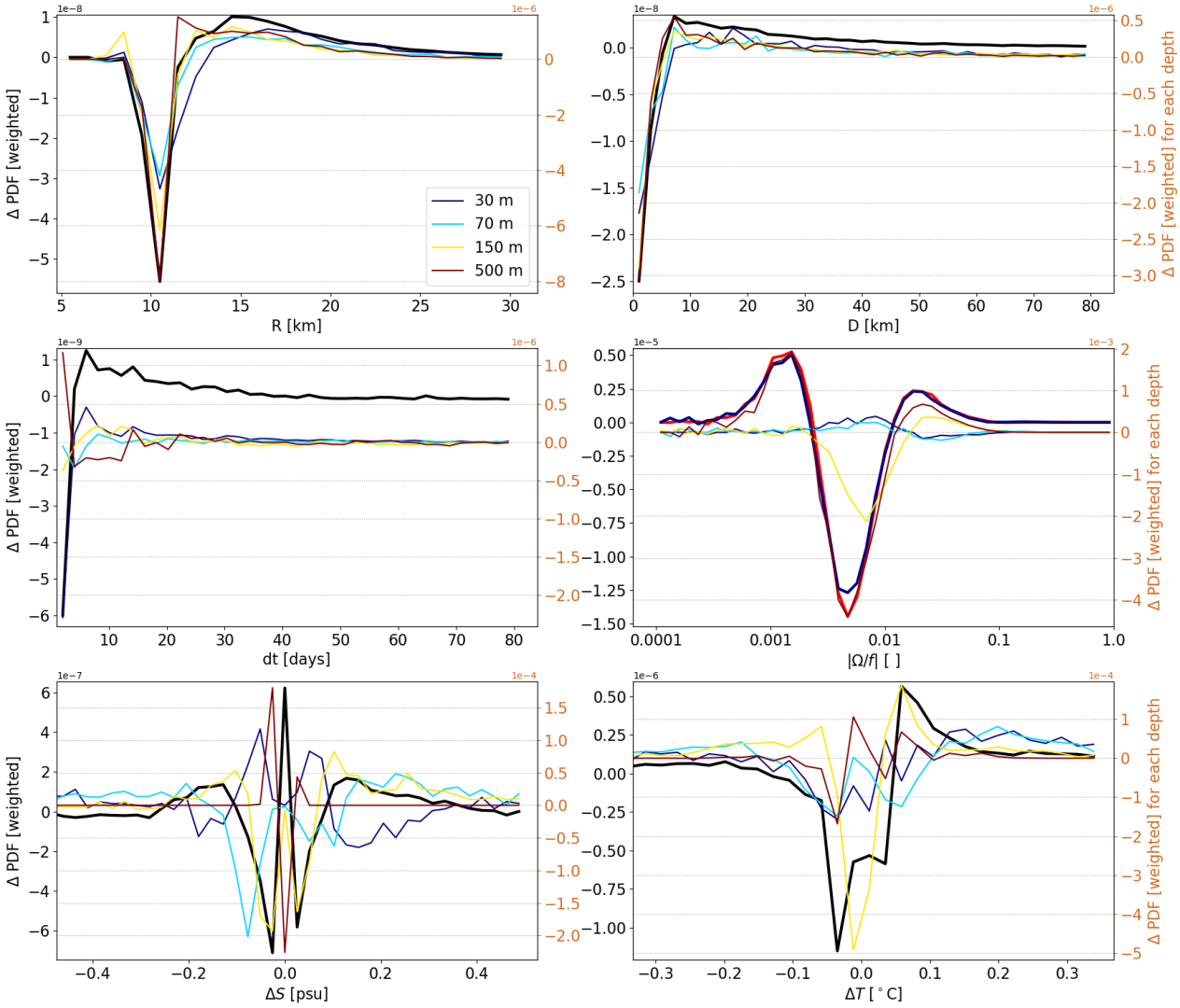

Figure 10. Difference between histograms of eddy properties at the end of the period (2015-2020) and at the beginning of the period (1995-2000), each histogram being weighted to remove the signature of the overall increase in the number of eddies. Black plain lines represent the statistics for all eddies aggregated between the surface and 1500 m, thin colored lines represent separately statistics at each depth. Red (resp. blue) plain thick lines represent the intensity of the anticyclonic (resp. cyclonic) eddies.

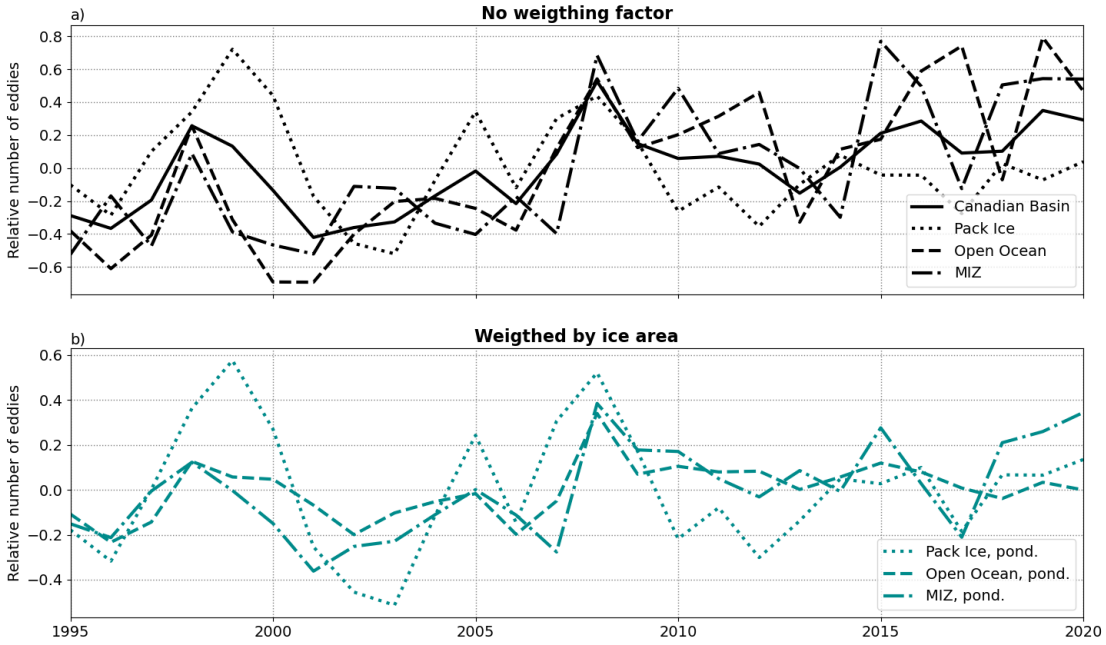

Figure 11. Time series of the relative number of eddies generated within the Canadian Basin in the upper layer for the three sea ice regions : Open Ocean (dashed lines), MIZ (dash-dotted lines) and Pack ice (dotted lines). The time series are weighted (b, respectively not weighted on panel a) by the yearly cumulated ice area of each region.

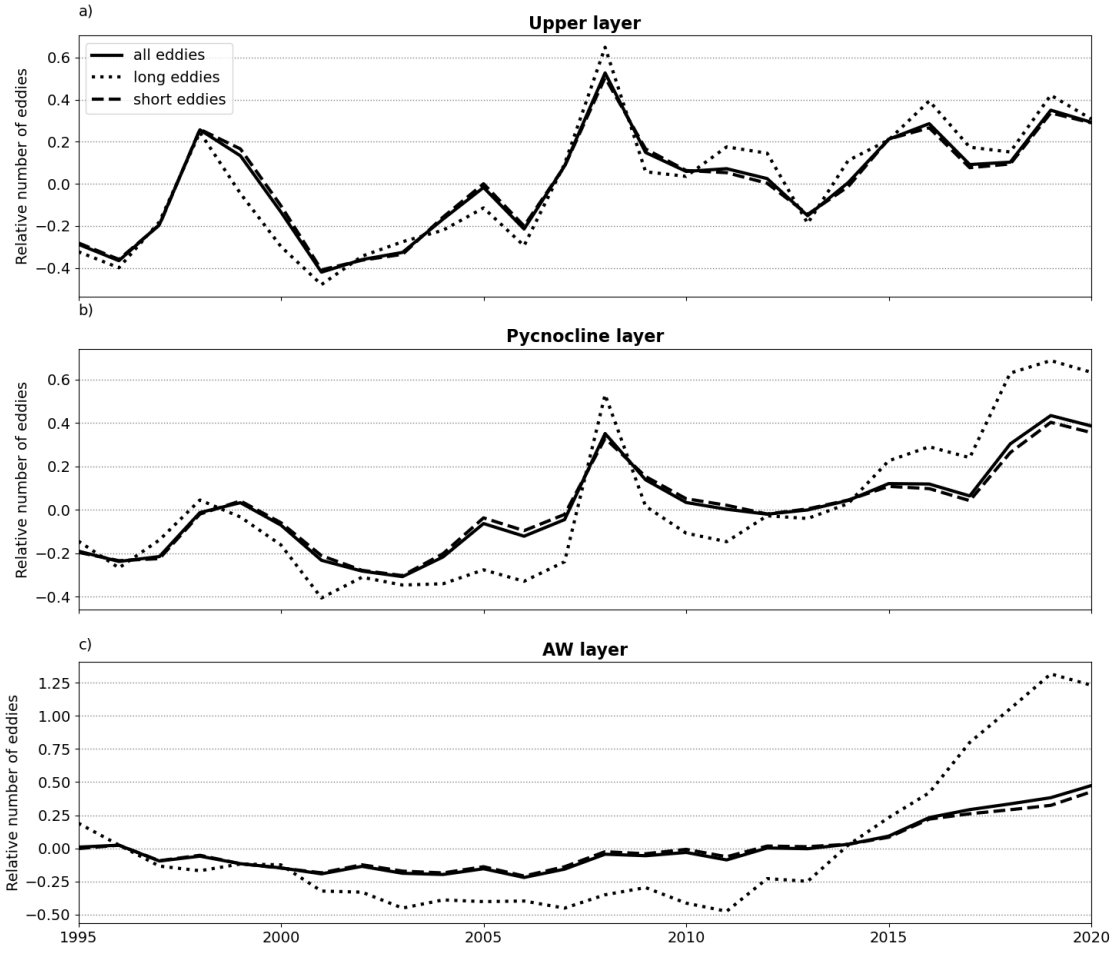

Figure 12. Time series of the relative number of eddies generated within the Canadian Basin for (a) the upper layer, (b) the pycnocline layer and (c) the AW layer, for respectively the short eddies (dashed lines), long eddies (dotted lines) and for all eddies (plain lines).

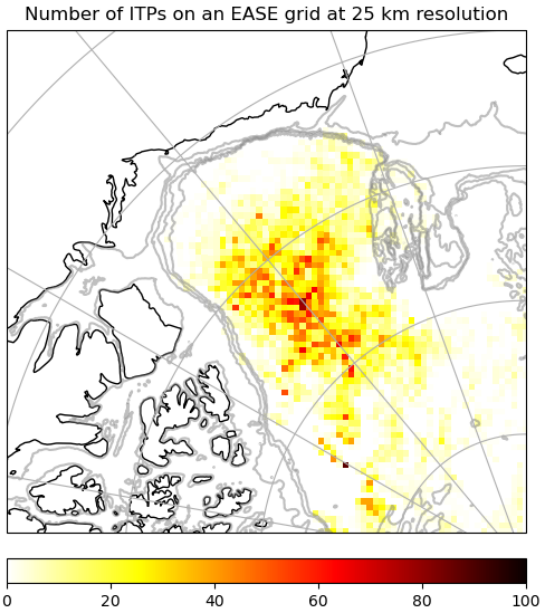

Figure 13. Number of ITP profiles available per Equal-Area Scalable Earth grid cell for an EASE grid of 25 km large. All ITPs processed to level-3 of post-processing between 2003 and 2024 are included and binned per day (Toole et al., 2011). We compute an occupation ratio for the ITP dataset on an Equal-Area Scalable Earth grid of 25 km large. We include all ITPs processed to level-3 of post-processing between 2003 and 2024 (Toole et al., 2011) and the profiles are binned per day. The occupation is computed for each grid cell, as the number of profiles by the total number of profiles.

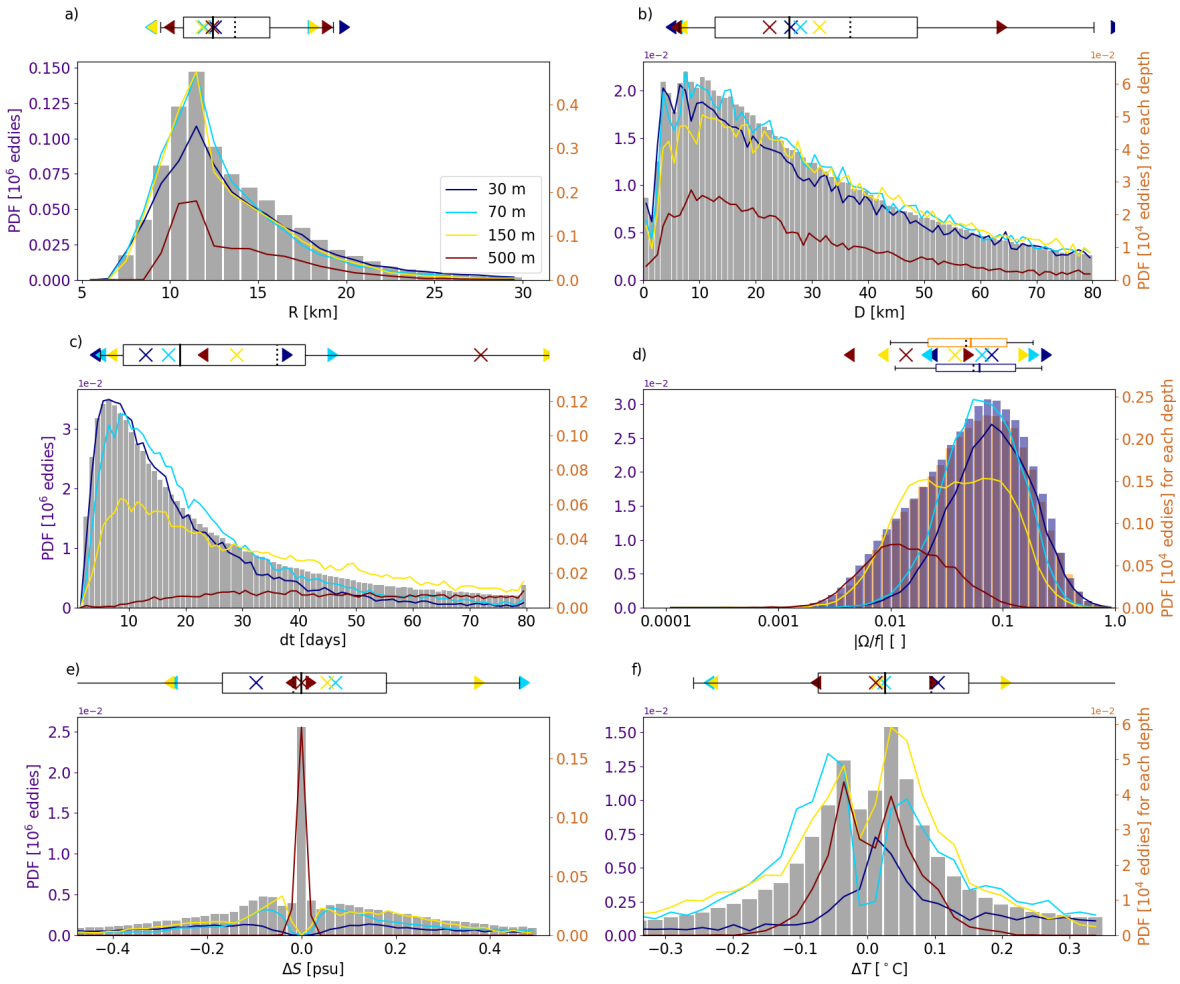

Figure 14. Same as Fig. 4 for long-lived eddies only : Histogram of the properties of eddies generated at all depths in the model: (a) radius, (b) distance travelled, (c) duration, (d) relative intensity for cyclones (blue) and anticyclones (orange), and anomalies in (e) salinity and (f) temperature with respect to the surrounding environment (see Sect. 2). All variables are estimated at the time of eddy generation, that is the first time an eddy is detected. Number of eddies are reported in million along the left axis (indigo). Anomalies are only accounted for when significant (see Sect. 2), that is only $\approx 15\%$ of the eddy population is considered for panels (e) and (f). Box plots indicate the quartiles Q1 and Q3, the median (plain line) and mean (dotted line), and the 10^{-th} and 90^{-th} percentiles in the whiskers. Plain lines correspond to the histogram of properties at specific depths (11 m, 30 m, 69 m, 147 m and 508 m), reported along the right axis in tens of thousands of eddies (orange). On panel d), plain lines report the histogram of absolute relative intensity, that is, for both cyclones and anticyclones together. Coloured ◄, ► and × respectively indicate the 10^{-th}, 90^{-th} and median at the corresponding depth.